

upstreamFoam: an OpenFOAM-based solver for heterogeneous porous media at different scales

Roberto Lange^a, Gabriel M. Magalhães^a, Franciane F. Rocha^{a,*}, Pedro V. S. Coimbra^a, Jovani L. Favero^a, Rodrigo A. C. Dias^a, Antonio O. S. Moraes^a, Mateus P. Schwalbert^b

^aWIKKI Brasil LTDA, Rua Aloísio Teixeira, 278, Prédio 3 - sala 301, Ilha da Cidade Universitária, Rio de Janeiro, 21941-850, RJ, Brazil

^bPetrobras Research Center (CENPES), Av. Horácio Macedo 950, Cidade Universitária, Ilha do Fundão, Rio de Janeiro, 21941-598, RJ, Brazil

Abstract

This is the preprint version of the published manuscript <https://doi.org/10.1016/j.ijmultiphaseflow.2024.104954>. Please cite as:

Lange, R.; Magalhães, G.M.; Rocha, F.F.; Coimbra, P.V.S.; Favero, J.L.; Dias, R.A.; Moraes, A.O.S; Schwalbert, M.P., 2024. Development of a new computational solver for multiphase flows in heterogeneous porous media at different scales. *International Journal of Multiphase Flow*, 104954.

This work presents the development of a novel solver tailored for simulating multiphase flows within heterogeneous porous media. Leveraging the Eulerian multi-fluid model coupled with Darcy's law, the solver demonstrates adaptability across diverse scales, effectively handling heterogeneous porosity and permeability fields. The proposed solver, called *upstreamFoam*, extends the capabilities of OpenFOAM framework, specifically the *multiphaseEulerFoam*, by incorporating models for porous media simulations. This integration introduces new features and formulations, allowing for the simulation of compressible multiphase flows in porous media with intricate properties. The approach presented here provides a robust framework for characterizing reservoirs and treating heterogeneous porous systems at different scales. A successful validation of the introduced solver for classical problems with analytical, semi-analytical, and reference solutions is presented. Then, applications on a wide range of multiphase flows in heterogeneous porous media at different scales have been studied, demonstrating the potential of the solver

to simulate complex multiphase problems.

Keywords: Multiphase flow, Porous media, Finite volume, OpenFOAM

1. Introduction

Multiphase flows describe several problems with applications in various fields. The Computational Fluid Dynamics (CFD) approaches have been extensively used for multiphase flows modeling and simulation (Spalding, 1981). Implementation of methodologies for solving CFD problems within open-source simulators is gaining popularity in industrial and academic research groups. The OpenFOAM library is an example, which is based on the Finite Volume Method (FVM) and covers a variety of cases (Jasak, 1996; Weller et al., 1998).

A well-known procedure for solving CFD problems is the Eulerian multi-fluid model (Hill, 1998; Ishii and Hibiki, 2010), which describes a system of phase fractions represented by averaged conservation equations (Crowe et al., 2012; Drew and Passman, 2006). In this context, work of Weller (2002) should be highlighted, where a conservative and bounded formulation based on a volumetric average for the momentum exchange terms has been presented.

There are different solution procedures for multiphase flow problems available in OpenFOAM. In the framework of Eulerian fluid models, the solver *twoPhaseEulerFoam* has been proposed, initially to simulate incompressible two-phase flows (Rusche, 2003). Silva et al. (2008) included the effects of particle-particle interaction by coupling the population balance equation with the *twoPhaseEulerFoam*. Then, the solver was extended to $n + 1$ phases, considering a continuous phase and n dispersed phases (Silva and Lage, 2011; Favero et al., 2015). Another solver, the *multiphaseEulerFoam*, has been developed to combine the Eulerian multi-fluid solution framework with the

*Corresponding author

Email addresses: roberto.lange@wikki.com.br (Roberto Lange), gabriel.magalhaes@wikki.com.br (Gabriel M. Magalhães), franciane.rocha@wikki.com.br (Franciane F. Rocha), pedro.coimbra@wikki.com.br (Pedro V. S. Coimbra), jovani.favero@wikki.com.br (Jovani L. Favero), rodrigo.dias@wikki.com.br (Rodrigo A. C. Dias), antonio.samel@wikki.com.br (Antonio O. S. Moraes), mateusps@petrobras.com.br (Mateus P. Schwalbert)

Volume of Fluid (VOF) method for interface capturing on selected phase pairs (Wardle and Weller, 2013). The proposed hybrid multiphase CFD solver employs the interface compression methodology of Weller (2008). The *multiphaseEulerFoam* considers a system of any number of compressible fluid phases with a common pressure, but with other separate properties. This approach allows for solving complex flows with multiple species, heat and mass transfer, being widely used (Tocci, 2016).

A wide range of multiphase flow applications occurs within porous media (Bear, 1988). The subsurface flows in oil reservoirs are relevant examples of such topics (Aziz, 1979). In the last years, several computational models for simulating multiphase flows in porous media have been introduced (Chen et al., 2006). An increase in the development of open-source simulators for this class of problems is also noticeable.

Regarding the OpenFOAM approach, a remarkable toolbox to simulate incompressible two-phase flows in porous media, called *porousMultiphaseFoam*, has been introduced by Horgue et al. (2015). This development includes a formulation for the phase saturations, relative permeability and capillary models, and special boundary conditions. Extensions of the *porousMultiphaseFoam* include an approach for adaptive mesh refinement (Sugumar et al., 2020) and a generalization for the black oil model (Fioroni et al., 2021). Recent developments have been presented by Horgue et al. (2022), such as improved numerical techniques for hydrogeological flows modeling and the transport problem of a mixture with n components. The *porousMultiphaseFoam* has also been used as the basis for the development of a hybrid approach to simulate two-phase flows in systems containing solid-free regions and porous matrices (Carrillo et al., 2020), besides that a two-phase flow procedure coupled with geomechanics and Embedding Discrete Fracture Model (EDFM) (Sangnimmuan et al., 2021).

In this paper, we develop a solver for multiphase flows in porous media combining the Eulerian multi-fluid formulation for a system of phase fractions with the Darcy's law for flows through porous media (Muskat, 1981). The mathematical model considers a locally averaged Navier-Stokes equation (Weller, 2002; Rusche, 2003) with an additional momentum source term, the Darcy term, considered to represent the porous domain and the effects related to permeability field, capillarity, and viscous forces. Since this type of modified Navier-Stokes system avoids the explicit treatment of the boundary conditions at the fluid and porous interface, it has been extensively used to simulate porous media flows (Goyeau et al., 2003). We can men-

tion other related approaches, generally used to solve flow problems through porous and solid-free regions simultaneously, such as the Darcy-Brinkman model (Brinkman, 1949), that uses a spatially dependent penalization term within the Navier-Stokes fluid momentum equation. More recently, a hybrid scale Darcy-Brinkman-based modeling framework, called micro-continuum approach, has been presented by Soulaire and Tchelepi (2016), and then extended by Carrillo et al. (2020). Another usual strategy is the definition of a mask function to set both porous areas with Darcy and Forchheimer coefficients (Forchheimer, 1901), and free areas where the classical Navier-Stokes momentum equation is solved. It is also very common to find works in the literature that solve mass conservation equations for each fluid with velocities expressed by Darcy’s law instead of solving a modified Navier-Stokes equation (Wu, 2015). However, we choose to use a more complete set of governing equations that may benefit future extensions.

The implementation of the proposed approach, in OpenFOAM, is based on the very used *multiphaseEulerFoam*, that has the capability to simulate a system of any number of compressible phase fractions at a common pressure, with the possibility of adding multiple species and mass transfer. We included the Darcy term for porous media modeling to the classic Navier-Stokes equation considered in the *multiphaseEulerFoam*, enabling it to be used for applications in porous media systems. In this new scenario, specialized models for reservoir simulation, such as those considered in *porousMultiphaseFoam*, are needed. We take advantage of the treatment for the relative permeability, capillarity models, and specific boundary conditions introduced by the *porousMultiphaseFoam*. Additionally, we incorporate new features and formulations, such as heterogeneous porosity fields, compressibility models, the definition of stationary phases, and the possibility of using more than two moving phases. Hence, the proposed solver, called *upstreamFoam*, extends the capabilities of the *multiphaseEulerFoam* and *porousMultiphaseFoam* to a greater variety of applications. A distinguishing property of the method presented here is the formulation of the solid as a stationary phase, which allows for the use of different minerals or different types of solids. With the new toolbox, we can handle complex simulations of compressible multiphase flows in porous media with intricate properties, which cannot be simulated independently in the previous solvers. Comparisons between *upstreamFoam* and *porousMultiphaseFoam* are presented in the numerical section for some porous media problems.

The multiphase porous media model requires the solution of a system of

coupled nonlinear partial differential equations. The numerical formulation adopted approximates the solution by a sequential scheme based on IMplicit Pressure Explicit Saturation (IMPES) (Coats, 2000), where the global mass conservation, expressed by a pressure equation, is implicitly solved, while the phase fractions are explicitly solved. More specifically, the segregated algorithm considered applies an external Pressure IMplicit with splitting of operator for Pressure-Linked Equations (PIMPLE) loop for pressure-velocity coupling (Wang et al., 2018) at each time step to approximate the problems of flow and transport. Inside the PIMPLE loop, the phase fractions are solved explicitly using the Multidimensional Universal Limiter with Explicit Solution (MULES) (Damián and Nigro, 2014), an OpenFOAM implementation of the Flux Corrected Transport (FCT) theory (Rudman, 1997). Due to the explicit treatment, the time steps need to satisfy the Courant-Friedrichs-Lewy (CFL) condition (Courant et al., 1928). In the numerical formulation section, we show two classic criteria for the time step choice implemented in *upstreamFoam*: the Courant condition (Courant et al., 1928), and the Coats restriction (Coats, 2003). Furthermore, details on reservoir characterization are highlighted, the relationship between the formulation based on phase fractions and other common approaches based on saturations is discussed, and the models considered for relative permeability, capillary pressure, and compressibility are presented.

The paper is divided into sections as follows. In section 2, the mathematical model is presented, followed by the numerical formulation in section 3, numerical results in section 4, and conclusions in section 5.

2. Mathematical Model

The Eulerian multi-fluid model considered in this work is given by volume averaged Navier-Stokes equations as presented by Weller (2002) and Rusche (2003). Since the main purpose of this work is to develop an application in OpenFOAM for multiphase flows in porous media to be used on oil and gas industry simulations, an additional Darcy term is used to account the porous media effects. Therefore, the mathematical formulation is presented with a particular emphasis on incorporating treatment for porous media.

The mathematical model considers that each volume contains both solid and void space. The void space, in turn, can contain multiple fluids. In the next subsections, porous media definitions and conservation principles that describe flows in porous media are presented.

2.1. Porous media definitions

The void space of a porous medium is represented by the porosity field

$$\alpha_v = \frac{V_v}{V}, \quad (1)$$

where V_v is the volume occupied by the void space and V is the volume of the respective cell, that is, the porosity is the void fraction and satisfies $0 \leq \alpha_v \leq 1$, where $\alpha_v = 0$ indicates an impermeable medium and $\alpha_v = 1$ a totally free region. We consider a system of phase fractions α_i , in which the index i represents one phase of the flow, such that for each cell

$$\alpha_i = \begin{cases} 0, & \text{cell does not contain phase } i, \\]0, 1[, & \text{cell contains phase } i \text{ and other phases,} \\ 1, & \text{cell is completely filled with phase } i. \end{cases} \quad (2)$$

Phase fractions satisfy the following relationship

$$\sum_{i=1}^{N_s} \alpha_i + \sum_{i=1}^{N_m} \alpha_i = 1, \quad (3)$$

where N_s is the number of stationary phases and N_m is the number of moving phases of the system. The total number of phases is denoted by $N = N_s + N_m$. In terms of the void fraction we have

$$\alpha_v = 1 - \sum_{i=1}^{N_s} \alpha_i. \quad (4)$$

It is important to notice that the solid is treated as a stationary phase, allowing to define different minerals or different types of solid as different stationary phases. Another advantage of this formulation is the possibility of considering residual saturations or particulate obstructions as stationary phases inclusively, allowing for the mass transfer between phases. In a numerical view, the solution of stationary phases is cheaper than the solution of moving phases.

Formulations based on saturations are more common than the phase fractions approach, however, the relationship between both consists in the fact that the saturation of a phase can be written as

$$S_i = \frac{\alpha_i}{\alpha_v}. \quad (5)$$

2.2. Balance equations

In the context of porous media flows, the phase momentum balance equation of each phase fraction is given by:

$$\frac{\partial(\alpha_i \rho_i \mathbf{u}_i)}{\partial t} + \nabla \cdot (\alpha_i \rho_i \mathbf{u}_i \mathbf{u}_i) = -\alpha_i \nabla p_i + \alpha_i \rho_i \mathbf{g} - \alpha_i^2 \frac{\mu_i}{k_{r,i}} \mathbf{K}^{-1} \mathbf{u}_i + \mathbf{F}_i, \quad (6)$$

in which, \mathbf{u}_i is the velocity of the phase i , ρ_i is the density of phase, p_i is the pressure of the phase, \mathbf{g} is the gravity acceleration, μ_i is the dynamic viscosity of the phase, $k_{r,i}$ is the phase relative permeability, \mathbf{K} is the absolute permeability tensor, and \mathbf{F}_i is a source term to account for additional effects. The above equation represents a complete momentum balance equation, that can consider turbulent stress, interfacial forces, and surface tension through the term \mathbf{F}_i (Weller, 2002; Rusche, 2003). Worth mentioning that the Darcy term containing permeability effects is dominant in the cases studied here (Muskat, 1981). Moreover, we highlight that the current formulation share similarities with the general modeling framework based on Darcy-Brinkman-Stokes equation presented by Soulaïne and Tchelepi (2016).

The pressure gradient ∇p_i can be replaced using a modified pressure p_i^* as follows:

$$\nabla p_i = \nabla p_i^* + \nabla (\rho_m (\mathbf{g} \cdot \mathbf{h})), \quad (7)$$

where the term $\rho_m (\mathbf{g} \cdot \mathbf{h})$ represents a pseudo-hydrostatic pressure, \mathbf{h} is the height of the fluid particle, and ρ_m is the fluid mixture density, defined as

$$\rho_m = \sum_{i=1}^{N_m} \alpha_i \rho_i. \quad (8)$$

Substituting Eq. (7) in Eq. (6) and rearranging, yields:

$$\begin{aligned} \frac{\partial(\alpha_i \rho_i \mathbf{u}_i)}{\partial t} + \nabla \cdot (\alpha_i \rho_i \mathbf{u}_i \mathbf{u}_i) = & -\alpha_i \nabla p_i^* + \alpha_i (\rho_i - \rho_m) \mathbf{g} - \alpha_i (\mathbf{g} \cdot \mathbf{h}) \nabla \rho_m \\ & - \alpha_i^2 \frac{\mu_i}{k_{r,i}} \mathbf{K}^{-1} \mathbf{u}_i + \mathbf{F}_i. \end{aligned} \quad (9)$$

The mass balance equation for each phase reads:

$$\frac{\partial(\alpha_i \rho_i)}{\partial t} + \nabla \cdot (\alpha_i \rho_i \mathbf{u}_i) = q_i, \quad (10)$$

where q_i is the source term related to the phase i . Equation (10) can be expanded and rewritten as

$$\frac{\partial \alpha_i}{\partial t} + \nabla \cdot (\alpha_i \mathbf{u}_i) = \frac{q_i}{\rho_i} - \frac{\alpha_i}{\rho_i} \frac{D_i \rho_i}{Dt}, \quad (11)$$

where the material derivative of ρ , which accounts for the compressibility effects, is given by

$$\frac{D \rho_i}{Dt} = \frac{\partial \rho_i}{\partial t} + \mathbf{u}_i \cdot \nabla \rho_i. \quad (12)$$

Another important concept is the mixture velocity \mathbf{u}_m which, for N phases, is given by

$$\mathbf{u}_m = \sum_{i=1}^N \alpha_i \mathbf{u}_i. \quad (13)$$

Moreover, the relative velocity between two phases i and j is defined as

$$\mathbf{u}_{r,ij} = \mathbf{u}_i - \mathbf{u}_j. \quad (14)$$

Then, summing the mass conservation equations of all phases and using the relation of Eq. (3), the total mass conservation can be written as

$$\nabla \cdot \mathbf{u}_m = \sum_{i=1}^N \frac{q_i}{\rho_i} - \sum_{i=1}^N \frac{\alpha_i}{\rho_i} \frac{D_i \rho_i}{Dt}. \quad (15)$$

Considering the concepts of mixture velocity and relative velocity, it is possible to express the general transport equation for each phase fraction α_i as

$$\begin{aligned} \frac{\partial \alpha_i}{\partial t} + \nabla \cdot (\alpha_i \mathbf{u}_m) + \sum_{\substack{j=1 \\ j \neq i}}^N (\nabla \cdot (\alpha_i \alpha_j \mathbf{u}_{r,ij})) &= \frac{q_i}{\rho_i} + \alpha_i \nabla \cdot \mathbf{u}_m \\ &- \frac{\alpha_i}{\rho_i} \frac{D_i \rho_i}{Dt} + \alpha_i \sum_{j=1}^N \frac{\alpha_j}{\rho_j} \frac{D_j \rho_j}{Dt}. \end{aligned} \quad (16)$$

Equation (16) was obtained following the conservative formulation for phase continuity equations developed by Weller (2002), Silva and Lage (2011), and Keser et al. (2021).

2.2.1. Capillary effects

The discontinuity between two moving phases of a multiphase flow on porous media generates an additional relationship between pressure fields denominated as capillary pressure p_c , given by:

$$p_{c,ki} = p_k^* - p_i^*, \quad (17)$$

in which k is a reference phase and i is any other phase of the system.

Using the definition of capillary pressure in Eq. (17) to replace the pressure of phase p_i^* in Eq. (9), one can write:

$$\begin{aligned} \frac{\partial(\alpha_i \rho_i \mathbf{u}_i)}{\partial t} + \nabla \cdot (\alpha_i \rho_i \mathbf{u}_i \mathbf{u}_i) = & -\alpha_i \nabla p_k^* + \alpha_i \nabla p_{c,ki} + \alpha_i (\rho_i - \rho_m) \mathbf{g} \\ & - \alpha_i (\mathbf{g} \cdot \mathbf{h}) \nabla \rho_m - \alpha_i^2 \frac{\mu_i}{k_{r,i}} \mathbf{K}^{-1} \mathbf{u}_i + \mathbf{F}_i. \end{aligned} \quad (18)$$

Therefore, the pressure of any phase i is defined as a function of the pressure of the reference phase k and the capillary pressure of the pair ki . Note that for the reference phase, the capillary pressure satisfies $p_{c,kk} = 0$, and hence Eq. (9) does not change.

2.3. Summary of the formulation

In summary, the mathematical model for compressible multiphase flows in porous media, explained above, consists of a set of partial differential equations, namely the momentum balance equation for each phase fraction, Eq. (18), a total mass balance equation, Eq. (15), and the transport equation of each phase fraction, Eq. (16):

$$\begin{aligned}
\frac{\partial(\alpha_i \rho_i \mathbf{u}_i)}{\partial t} + \nabla \cdot (\alpha_i \rho_i \mathbf{u}_i \mathbf{u}_i) &= -\alpha_i \nabla p_k^* + \alpha_i \nabla p_{c,ki} + \alpha_i (\rho_i - \rho_m) \mathbf{g} \\
&\quad - \alpha_i (\mathbf{g} \cdot \mathbf{h}) \nabla \rho_m - \alpha_i^2 \frac{\mu_i}{k_{r,i}} \mathbf{K}^{-1} \mathbf{u}_i + \mathbf{F}_i \\
\nabla \cdot \mathbf{u}_m &= \sum_{i=1}^N \frac{q_i}{\rho_i} - \sum_{i=1}^N \frac{\alpha_i}{\rho_i} \frac{D_i \rho_i}{Dt} \\
\frac{\partial \alpha_i}{\partial t} + \nabla \cdot (\alpha_i \mathbf{u}_m) + \sum_{\substack{j=1 \\ j \neq i}}^N (\nabla \cdot (\alpha_i \alpha_j \mathbf{u}_{r,ij})) &= \frac{q_i}{\rho_i} + \alpha_i \nabla \cdot \mathbf{u}_m \\
&\quad - \frac{\alpha_i}{\rho_i} \frac{D_i \rho_i}{Dt} + \alpha_i \sum_{j=1}^N \frac{\alpha_j}{\rho_j} \frac{D_j \rho_j}{Dt}.
\end{aligned} \tag{19}$$

In the next section, we detail the numerical treatment for approximating and solution of the model system of equations Eq. (19).

3. Numerical Formulation

In this section, we describe the algorithm used to solve the nonlinear system for multiphase flows in porous media along with some models considered and their particularities.

3.1. Solution approach

A segregated scheme based on IMPES (Coats, 2000) is considered, where the global mass conservation, expressed by a pressure equation, is implicitly solved, while the phase fractions are explicitly solved.

The numerical model has been implemented in the OpenFOAM framework, that uses the following notation for the momentum balance equation after receiving a finite-volume discretization

$$\mathbf{A}_i \mathbf{u}_i = \mathbf{H}_i(\mathbf{u}_i) - \alpha_i \left(\nabla p_k^* - \nabla p_{c,ki} - (\rho_i - \rho_m) \mathbf{g} + (\mathbf{g} \cdot \mathbf{h}) \nabla \rho_m \right), \tag{20}$$

where \mathbf{A}_i represents the diagonal term of the matrix system and \mathbf{H}_i represents the off-main diagonal portion of the coefficient matrix with the source term \mathbf{F}_i added.

In order to write a system for pressure and phase fractions, Eq. (20) is divided by the diagonal coefficient and \mathbf{u}_i is substituted into the total mass conservation Eq. (15), resulting in the following expression:

$$\nabla \cdot \left[\sum_{i=1}^N \frac{\alpha_i}{\mathbf{A}_i} \left(\mathbf{H}_i(\mathbf{u}_i) - \alpha_i \left(\nabla p_k^* - \nabla p_{c,ki} - (\rho_i - \rho_m) \mathbf{g} + (\mathbf{g} \cdot \mathbf{h}) \nabla \rho_m \right) \right) \right] = \sum_{i=1}^N \frac{q_i}{\rho_i} - \sum_{i=1}^N \frac{\alpha_i}{\rho_i} \frac{D_i \rho_i}{Dt}. \quad (21)$$

Note that only one pressure equation is obtained for the system instead of a pressure equation for each phase. The total flux ϕ resulting from the pressure equation receive the contributions

$$\phi = \phi_p + \phi_{p_c} + \phi_g, \quad (22)$$

where ϕ_p , ϕ_{p_c} , and ϕ_g represent the flux generated, respectively, by the pressure gradient, capillary pressure and gravity driving forces. The reformulated system is in agreement with the basic framework of OpenFOAM for velocity and pressure coupling. To approximate the pressure-velocity coupling, a solver based on Pressure IMPLICIT with splitting of operator for Pressure-Linked Equations (PIMPLE) available in OpenFOAM is used (Wang et al., 2018).

The phases fractions, in turn, are solved explicitly using the Multidimensional Universal Limiter with Explicit Solution (MULES) (Damián and Nigro, 2014), an OpenFOAM implementation of the Flux Corrected Transport (FCT) theory (Rudman, 1997).

As a classic finite volume-based numerical scheme, our solver considers the variables calculated in the cell center and interpolated to the faces if necessary. The *upstreamFoam* has an additional option of constructing term by term of the momentum equation interpolated on the faces of the control volumes. This option increases the numerical stability and accuracy of the balance of forces. To interpolate the different variables distinct numerical schemes are used, for example, linear interpolation, first-order upwind scheme, and harmonic average. More details about the discretization procedures in OpenFOAM can be found in seminal works of Jasak (1996) and Weller et al. (1998).

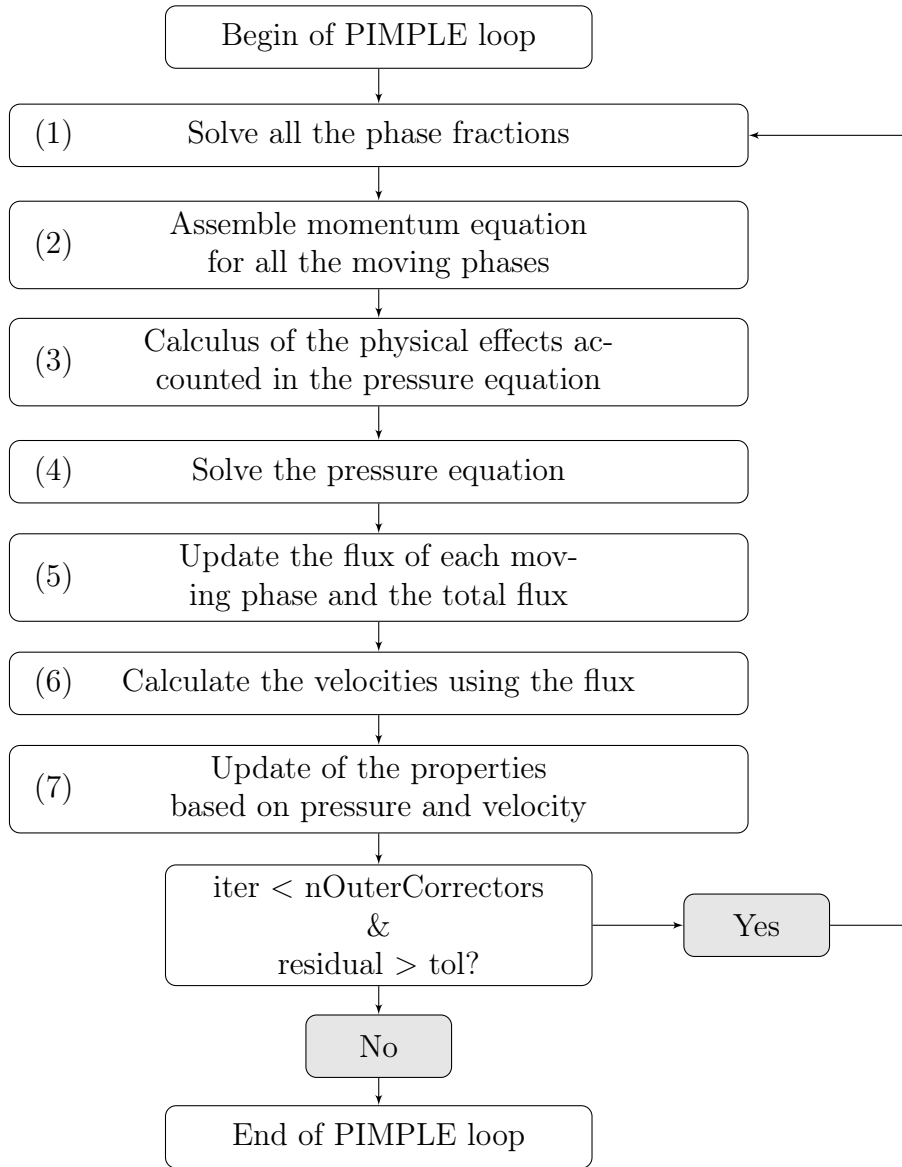


Figure 1: Flowchart of the external loop for one time step.

3.1.1. Algorithm

The numerical scheme applies an external PIMPLE loop at each time step to approximate the problems of flow and transport sequentially. Considering the PIMPLE algorithm (Wang et al., 2018; Greenshields and Weller, 2022) for pressure-velocity coupling, the flowchart of a PIMPLE loop in *upstreamFoam* is shown in Fig. 1, detailing the main operations. When the loop begins, all the phase fractions are solved (step 1). The MULES algorithm is used for the moving phases, while a diagonal solver is used for the stationary phases due to the simplicity of the mass balance when the phase is stationary.

Next, the momentum equation is assembled for all moving phases (step 2), noting that there is no momentum prediction in the *upstreamFoam* formulation. Since the phase fractions at faces are repeatedly used in subsequent steps, they are interpolated and stored in a new field for efficiency. The physical effects that must be accounted for in the pressure equation, such as gravitational effects, capillary pressure, compressibility, and dilatation, are calculated in step 3. Finally, the pressure equation is solved (step 4).

With the phase fractions and pressure solved, the flux of each moving phase and the total flux are updated (step 5). The velocities at the cell centers are then obtained (step 6) using the fluxes calculated in the previous step. Finally, with updated fields of phase fraction, pressure, and velocities, other properties based on these fields such that relative permeability, density and viscosity are updated. These seven steps are repeated until the tolerance, that is based on a residual related to the change in pressure solution, or the maximum number of iterations (`nOuterCorrectors`) is reached. We remark that if only one external iteration is defined, the algorithm falls back into a scheme similar to IMPES.

3.1.2. Time-step limitations

Due to the explicit treatment, the time steps need to satisfy the Courant-Friedrichs-Lewy (CFL) condition (Courant et al., 1928). Since there is no single optimal criterion always ensuring stability and efficiency (Franc et al., 2016), the *upstreamFoam* has two classic criteria for the time step choice: the Courant condition (Courant et al., 1928), and the Coats restriction (Coats, 2003). In the implemented models, the time step is adaptively adjusted such that the following limit is not exceeded:

$$\Delta t_{\max} = \frac{C_{\max}}{C}, \quad (23)$$

where C_{\max} is a user-defined limit and C is a restriction defined by each stability criterion according to the flow properties.

The classic Courant number condition is given by

$$C = C_{\text{Courant}} = \frac{1}{2} \max_{\alpha_i, j} \left(\frac{\sum_{f=1}^{m_j} |\phi_f|}{V_j} \right) \Delta t, \quad (24)$$

where ϕ_f are the total fluxes of phase fraction α_i through each face f of cell j , m_j is the total number of faces of cell j , V_j is the volume of cell j , and Δt is the previous time step.

The Coats criterion (Coats, 2003) is also considered by the *upstreamFoam*. We use a system containing a wetting phase w and a non-wetting phase n to describe this condition, which in this case is given by

$$C = C_{\text{Coats}} = \max_j \left[\frac{1}{\alpha_v V_j} \left(\Psi \frac{\partial p_c}{\partial S_w} \sum_{f=1}^{m_j} T_f + \frac{\partial F_w}{\partial S_w} \sum_{f=1}^{m_j} \phi_f \right) \right] \Delta t, \quad (25)$$

where T_f is the transmissibility of face f of cell j

$$T_f = \frac{K_f A_f}{\Delta x_f}, \quad (26)$$

A_f is the area of face f , Δx_f is the distance between the centers of two neighboring cells that contain face f , and K_f is the harmonic interpolation of absolute permeability at face f . Defining the phase mobilities $\lambda_i = k_{r,i}/\mu_i$, $i \in \{w, n\}$, one have that Ψ is the harmonic average of mobilities

$$\Psi = \frac{2\lambda_w \lambda_n}{\lambda_w + \lambda_n} \quad (27)$$

and F_w is the fractional flow

$$F_w = \frac{\lambda_w}{\lambda_w + \lambda_n}. \quad (28)$$

In Eq. (25), the evaluated ϕ_f considers the sum of the total fluxes of both phases through face f . Coats (2003) shows a formulation of the Coats criterion for a three-phase system.

Note that the Courant condition depends on fluxes of phases, while the Coats restriction considers the same fluxes and additional information related

to the fractional flow and capillary pressure effects. Therefore, the Coats stability criterion is more adapted to the porous media problems, however, it may be very restrictive in certain circumstances and is not necessarily the optimum choice (Franc et al., 2016). As both criteria are able to avoid numerical instabilities due to the non-linear effects involved in the problems considered in this paper, we control the time step variations by Coats restriction for the cases with capillary pressure and by Courant condition for the remaining cases. We refer to the comparative study by Franc et al. (2016) for more detailed discussions about the effectiveness of each criterion at different porous media flow regimes.

3.2. Porous media modeling

In this section, we describe the models used to deal with the essential features of multiphase flows in porous media.

3.2.1. Relative permeability models

A generic framework for multiphase flows with any number of phases requires relative permeability models with respect to each fluid. We apply the widely used Brooks and Corey model (Brooks, 1965), which relates the relative permeability of each phase to the phase fraction by

$$k_{r,i} = k_{r,i(\max)} \left(\frac{\alpha_i}{\alpha_v} \right)^n, \quad (29)$$

where n is a power coefficient associated to the porous media properties, and $k_{r,i(\max)}$ is the maximal relative permeability.

Relative permeability functions depend on the particular porous medium and fluid phases, and they are obtained by performing displacement experiments on samples that represent the real conditions of each porous medium, if possible. The same applies to the exponent of the Brooks and Corey model, which is usually obtained by fitting experimental data. However, there are some standard choices, for example, quadratic functions, whose application is adequate to represent the non-linear coupling between flow and transport in porous media (Aziz, 1979). It is worth noting that it is also possible to find equivalence between the parameters of the Brooks and Corey model to other models in the literature (Morel-Seytoux et al., 1996).

The *upstreamFoam* also allows for the use of tabulated methodology, considering a user provided table with the relative permeability value as a function of the saturation.

3.2.2. Capillary pressure models

We consider classical approximations that p_c depends only on saturation, and hence

$$\nabla p_c = p'_c \nabla \left(\frac{\alpha_i}{\alpha_v} \right). \quad (30)$$

A well-known correlation considered here for the capillary pressure is the Brooks and Corey model (Brooks, 1965), which is given by the following expression

$$p_c = p_{c,0} \left(\frac{\alpha_i}{\alpha_v} \right)^{-\beta}, \quad (31)$$

where $p_{c,0}$ is the entry capillary pressure and β is a parameter related to the pore size distribution.

An application of a user-defined table with capillary pressure derivative value as a function of the saturation is also possible. Another possibility is the computation of the capillary pressure through interpolations performed with tabulated data of the Leverett J-function (Leverett, 1941) provided by the user.

3.2.3. Compressibility models

To consider compressible phases, we assume that the density can be expressed in terms of the pressure through compressibility terms. For example, in the case of a compressible formation, the porosity, that is, the void fraction α_v , is a pressure dependent unknown.

A basic model considered for compressible flows computes the density variation according to a constant compressibility, such that:

$$\rho = \rho_0 e^{c(p-p_0)}, \quad (32)$$

where c is the compressibility of the phase, ρ_0 is a reference density, and p_0 is a reference pressure. It is derived from an equation of state and can be applied to most liquids that do not contain large amounts of dissolved gas (Chen et al., 2006). If the flow is slightly compressible, which corresponds to the cases considered in our experiments, it is enough to use the following linear approximation:

$$\rho = \rho_0 (1 + c(p - p_0)). \quad (33)$$

For gas flow, gas compressibility is generally not considered constant, and a form that considers the gas law is required (Aziz, 1979).

Other possibility available in *upstreamFoam* is the application of a user-defined table with density value as a function of the pressure. We remark that other models to simulate compressible moving phases implemented on the thermophysical classes of OpenFOAM (Nguyen et al., 2022) can be easily incorporated into the *upstreamFoam*.

4. Numerical Results

In this section, the multiphase model for flows in porous media is used in several experiments for verification and application in realistic data. Initially, we study classical problems by comparing the results obtained with analytical or semi-analytical solutions. Then, the solver is applied to approximate reservoir scale problems, including the realistic SPE10 benchmark (Christie and Blunt, 2001). To close, a multiphase flow simulation in a heterogeneous core is presented.

The main numerical schemes used in our experiments include explicit Euler time integration, linear discretizations for gradients, and the first-order upwind method for divergents. The linear system is solved with stabilized preconditioned conjugate gradient (PCG) method combined with a generalized geometric algebraic multigrid (GAMG) method and diagonal incomplete Cholesky (DIC) smoother considering a tolerance of 10^{-8} . The PIMPLE loop is defined with a tolerance of 10^{-4} and 10 outer iterations.

Extensive research has demonstrated significant improvements in the scalability and parallel performance of OpenFOAM in high-performance computing (HPC) environments. For instance, studies by Galeazzo et al. (2024a) have provided in-depth analyses of OpenFOAM’s performance on various HPC architectures, highlighting its capability to efficiently utilize modern computing resources. Given that *upstreamFoam* is fully based on OpenFOAM, its parallel performance is expected to align closely with that of the underlying framework. This implies that any advancements in OpenFOAM’s parallel efficiency will likely result in corresponding improvements in *upstreamFoam*. The speed-up results showed by Horgue et al. (2015) for an OpenFOAM-based toolbox for porous media confirm this behavior as it is observed a super linear speed-up in a certain range, aligned with the observation in the work of Galeazzo et al. (2024b).

As the primary objective of the current work is to present the formulation and validation of the implemented code, all the simulations in the following

sections were executed using just one core (serial) of an Intel Core i7-12700H processor CPU 4.7GHz with 64GB of memory.

4.1. Verification cases

We verify the solver using classical problems with analytical or semi-analytical solutions. Four cases are considered, the first and second ones are homogeneous and heterogeneous Buckley-Leverett problems, the third one is a capillary-gravity equilibrium, and the last one is a compressible formation case. The validation cases were chosen such that relative permeability, capillary-gravity forces, and compressibility effects can be evaluated separately. The objective is to verify whether the new solver produces results that converge to the reference solutions when applied to different situations since it will then be used to simulate realistic problems with all these effects.

4.1.1. Homogeneous Buckley-Leverett

The behavior of a two-phase immiscible and incompressible flow in one-dimensional porous medium can be investigated using the Buckley-Leverett semi-analytical solution (Wu, 2015).

In this study, we perform a numerical verification considering a channel of 0.065 m long saturated with oil (denoted by the subscript o), where water (denoted by the subscript w) is injected from left at a constant volumetric rate of 1.66×10^{-8} m/s, and the pressure at right is fixed in 0.1 MPa. This case considers homogeneous porosity of $\alpha_v = 0.2$ and absolute permeability of $\mathbf{K} = 1 \times 10^{-13}$ m². The gravity and capillary pressure are negligible. The phase densities are $\rho_w = 1000$ kg/m³ and $\rho_o = 800$ kg/m³, while the viscosities are $\mu_w = 0.001$ Pa·s and $\mu_o = 0.002$ Pa·s. The Brooks and Corey relative permeability model with $n = 2$ and $k_{r,i(\max)} = 1$ is applied for both phases. The Courant time step control is selected with $C_{\max} = 0.5$.

In Fig. 2 the saturation profile after 1800 s is shown for a computational mesh with 500 cells, where it is possible to note that the approximation is close to the analytical solution. A convergence study is reported in Table 1, where L^1 errors are compared for different meshes. We observe errors decreasing substantially in a linear behavior, that is the expected slope due to the first-order discretizations. Additionally, the execution times are shown.

4.1.2. Heterogeneous Buckley-Leverett

An extension of the previous analysis to flows in one-dimensional heterogeneous porous medium has been introduced by Wu (2015), in which the formation consists of a number of domains with different rock properties.

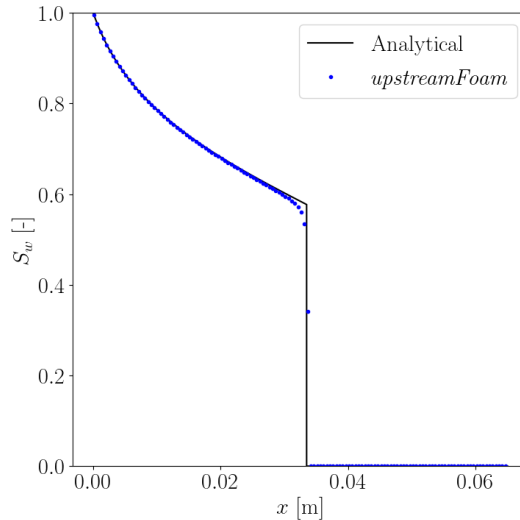


Figure 2: Saturation profile after 1800s of the homogeneous Buckley-Leverett case.

Number of cells [-]	L^1 error [-]	Execution time [s]
500	0.003637	1.21
1000	0.001968	3.14
2000	0.001022	9.26
4000	0.000370	31.35

Table 1: L^1 errors and execution times for the homogeneous Buckley-Leverett case.

In order to consider the heterogeneous case, we assume that the porosity is $\alpha_v = 0.2$ if $0 \leq x \leq 0.0325$, and $\alpha_v = 0.1$ if $0.0325 < x \leq 0.065$. In the Brooks and Corey relative permeability model, we consider $n = 1$ for both phases if $x \leq 0.325$ and $n = 4$ for both phases if $x > 0.325$. All the other parameters consider the same setup of the previous example.

In Fig. 3 the saturation profile after 1800s is shown for a computational mesh with 500 cells, where we also note that the approximation is close to the analytical solution for the heterogeneous case. Table 2 shows the respective convergence study, with errors decreasing as the mesh is refined. The behavior of the execution time when refining the mesh is also shown, where we can note an increase in the computational cost in relation to the homogeneous case.

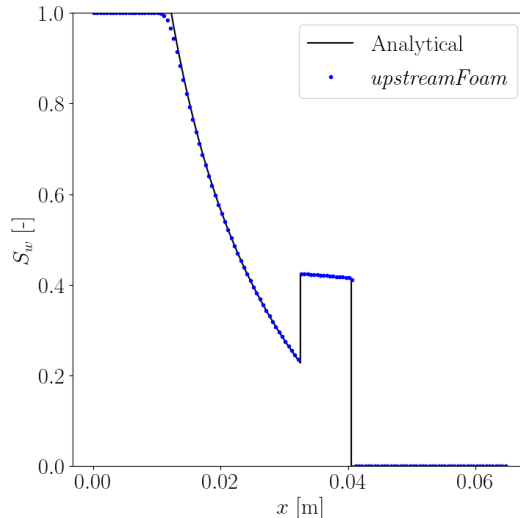


Figure 3: Saturation profile after 1800 s of the heterogeneous Buckley-Leverett case.

Number of cells [-]	L^1 error [-]	Execution time [s]
500	0.004342	1.96
1000	0.002499	5.25
2000	0.001416	16.40
4000	0.000889	58.84

Table 2: L^1 errors and execution times for the heterogeneous Buckley-Leverett case.

4.1.3. Capillary-gravity equilibrium

We now study an air-water incompressible flow in a vertical column (1 m tall) with capillary and gravity effects. The flow is carried out until the gravity-capillarity equilibrium, starting with an initial distribution of the water saturation in a step-wise fashion: the lower half is partially saturated with water ($S_w = 0.5$ and $S_a = 0.5$), while the upper half is dry ($S_w = 0$ and $S_a = 1$). The bottom boundary condition is a Neumann zero condition, and the top boundary condition is a Dirichlet fixed pressure of 0.1 MPa.

Homogeneous porosity of $\alpha_v = 0.2$ and absolute permeability of $\mathbf{K} = 1 \times 10^{-11} \text{ m}^2$ are considered. The phase densities are $\rho_w = 1000 \text{ kg/m}^3$ and $\rho_a = 1 \text{ kg/m}^3$, while the viscosities are $\mu_w = 0.001 \text{ Pa} \cdot \text{s}$ and $\mu_a = 1.76 \times 10^{-5} \text{ Pa} \cdot \text{s}$. The Brooks and Corey relative permeability model with $n = 1$ and $k_{r,i(\text{max})} = 1$ is applied for both phases. Moreover, the capillary pressure

is defined through a table filled by the Brooks and Corey correlation using 501 points with parameters $p_{c,0} = 1000$ Pa and $\beta = 0.5$. The Coats criteria has been applied, with $C_{\max} = 0.5$.

Following the analysis proposed by Horgue et al. (2015) and Carrillo et al. (2020), the theoretical steady state can be described as the balance between capillary and gravitational forces, described by

$$\frac{\partial p_c}{\partial y} = (\rho_a - \rho_w)g_y, \quad (34)$$

where $g_y = -9.8 \text{ m/s}^2$ is the gravity in the main flow direction. The expression above can be written as

$$\frac{\partial S_w}{\partial y} = \frac{(\rho_a - \rho_w)g_y}{\frac{\partial p_c}{\partial S_w}}, \quad (35)$$

which allows for the calculation of the water saturation gradient according to the chosen capillary pressure model.

The saturation profile at the capillary-gravity equilibrium (after 20000 s) for a computational mesh with 300 cells can be seen in Fig. 4(a). We remark that this case was presented by Horgue et al. (2015) for the development of the *porousMultiphaseFoam* toolbox. Therefore, a comparison between both approximations with equivalent numerical setup is included, specifically using the solver *impesFoam* available in *porousMultiphaseFoam*. It is possible to note that the obtained saturation profiles are related. A comparison between theoretical and numerical evaluations of the water saturation gradient can be seen in Fig. 4(b), in which we see that both solutions are very similar.

In Table 3, the convergence study along with computational times for the capillary-gravity test are presented. It is possible to note that the errors decrease as the mesh is refined, while the computational time is increased. Note that, due to the effect of capillary pressure, the computational cost for this experiment increased significantly compared to the previous examples. Furthermore, the *impesFoam* required a computational time of 401.01 s for the mesh with 300 cells, which corresponds to less than half the computational time required by the *upstreamFoam*. However, when comparing the computational time between *upstreamFoam* and *impesFoam* we need to keep in mind that the latter is a solver for two-phase flows with only constant porosity fields and without considering compressibility effects. In other words, the *upstreamFoam* proposal is not to be computationally faster than *impesFoam*,

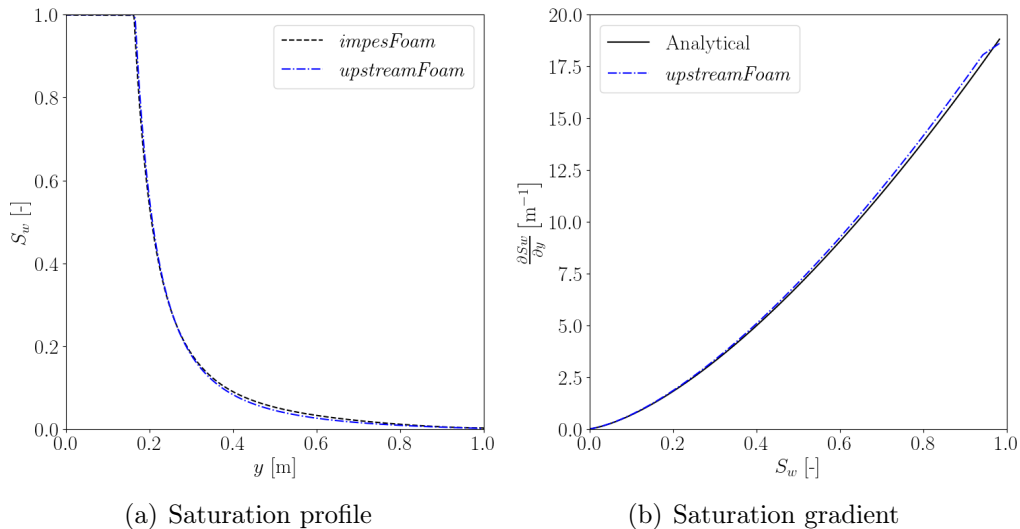


Figure 4: Capillary-gravity equilibrium test.

Number of cells [-]	L^1 error [-]	Execution time [s]
30	0.2413	7.88
75	0.09575	48.52
150	0.048429	227.1
300	0.042366	1000.86

Table 3: L^1 errors and execution times for the capillary-gravity equilibrium test.

but rather to add the modeling of physical complexities that enable a greater variety of applications.

4.1.4. Compressible formation

Since the formation compressibility can significantly influence the reservoir estimations, we propose a simplified verification of the total mass of oil produced in a scenario of depletion generated by compressibility effects. The present experiment considers an oil single-phase flow, however, the *upstreamFoam* framework performs the computation of both porous and fluid phases.

We study the flow of an incompressible oil in a one-dimensional compressible reservoir of 1000 m long with 100 computational cells. The reservoir, filled with oil, is initially under a pressure of 100 MPa, and a fixed pressure

of 10 MPa is maintained at the outlet, resulting in a transient state of oil production by system depletion. The initial porosity, that is, the initial void fraction of the system, is homogeneous, with a value of $\alpha_v = 0.3$. We consider a constant compressibility of $c_v = 1 \times 10^{-9} \text{ Pa}^{-1}$, absolute permeability of $\mathbf{K} = 1 \times 10^{-12} \text{ m}^2$, oil density of $\rho_o = 800 \text{ kg/m}^3$, and oil viscosity of $\mu_o = 0.002 \text{ Pa} \cdot \text{s}$. In this experiment, gravity effects are neglected.

Once the porous medium is compressible, the void fraction varies with pressure, and can be described by using a compressibility model, as for example,

$$\alpha_v = \alpha_{v,0} (1 + c_v(p_v - p_{v,0})), \quad (36)$$

where c_v is the compressibility of the formation, $\alpha_{v,0}$ is the reference porosity, and $p_{v,0}$ is the reference pressure. The above correlation allows for calculating a semi-analytical estimation for the mass balance between the initial and final states of the system.

Considering that the mass of the formation is conserved throughout the depletion process, the initial oil mass is $m_o^i = \alpha_v^i \rho_o V$, while the final oil mass is $m_o^f = \alpha_v^f \rho_o V$. Therefore, the total mass of oil produced, m_o^p , can be calculated by

$$m_o^p = m_o^i - m_o^f = (\alpha_v^i - \alpha_v^f) \rho_o V. \quad (37)$$

Using the linear model of Eq. (36) in Eq. (37), gives the following expression for the total mass of oil produced:

$$m_o^p = \alpha_{v,0} c_v (p_v^i - p_v^f) \rho_o V. \quad (38)$$

For the simulation parameters considered above, an oil production of $5.4 \times 10^7 \text{ kg}$, i.e., 424 562.18 STB after depletion is estimated. To evaluate the amount of produced mass of oil during the simulation, we test different values of time step size. The results are reported in Table 4, where it is possible to note that the solver produces adequate results with the error decreasing as the time step decreases.

The graph in Fig. 5 illustrates the curve of oil produced for $\Delta t = 150 \text{ s}$. Note that the calculated mass of oil produced approaches the expected value.

4.2. 2D reservoir problems

This section presents the application of *upstreamFoam* to approximate two reservoir scale problems. The first experiment shows the evaluation of the head loss of an oil flow in a circular reservoir. The second experiment presents a gas-oil flow in a heterogeneous reservoir with data given by the realistic SPE10 benchmark (Christie and Blunt, 2001).

Time step [s]	Oil produced [STB]	Error [%]
2400	411196.33	3.15
1200	415127.46	2.22
600	418272.36	1.56
300	419844.82	1.09
150	421417.27	0.75

Table 4: Mass of oil produced according to the time step size.

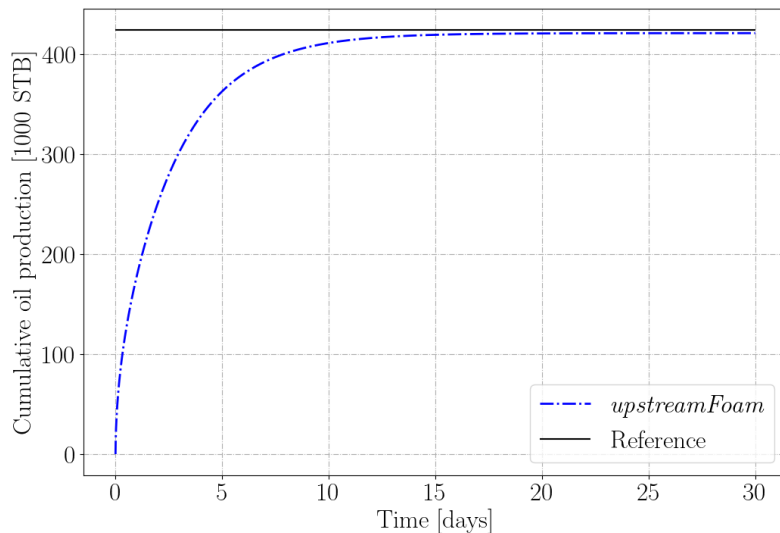


Figure 5: Mass of oil produced by the *upstreamFoam* with $\Delta t = 150$ s.

4.2.1. Oil flow in a circular reservoir

The head loss of the reservoir is a typical estimate in oil recovery studies. In this experiment, the head loss of a 2D reservoir with oil production by system depletion is investigated.

We simulate the flow of an incompressible oil in a compressible reservoir, given by a circular geometry. The reservoir is initially fully saturated with oil, which is produced through a sink term located in the center of the domain. A fixed pressure of 19.61 MPa is maintained at the boundaries, along with a constant flow rate of $q = 0.36 \times 10^{-4} \text{m}^3/\text{s}$ at the sink cell. The reservoir, with a diameter of 1000 m, contains an initial homogeneous void fraction of

$\alpha_v = 0.3$. Linear compressibility model is considered with $c_v = 1 \times 10^{-9} \text{ Pa}^{-1}$, absolute permeability of $\mathbf{K} = 2 \times 10^{-13} \text{ m}^2$, oil density of $\rho_o = 880 \text{ kg/m}^3$, and oil viscosity of $\mu_o = 0.002 \text{ Pa} \cdot \text{s}$. In this experiment, gravity effects are neglected. The Courant time step control is selected with $C_{\max} = 0.5$.

Figure 6 shows the pressure profile at time $t = 182.64$ days yielded by a simulation with 2053 computational cells. In this case, the cell size is $\Delta x = \Delta y = 19.6 \text{ m}$. From the pressure profile, it is noted that the flow is symmetrical towards the producing cell.

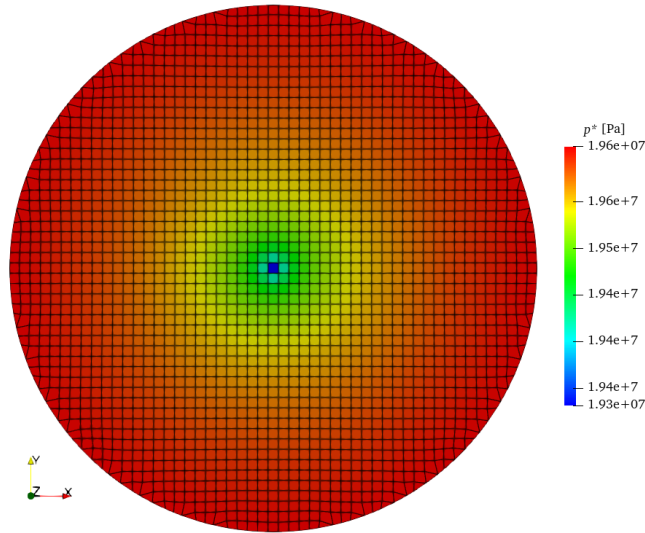


Figure 6: Pressure profile of the 2D reservoir with a sink cell in the center of the domain.

Considering a radial reservoir and using mass conservation and Darcy law for a single-phase flow, one can write

$$\frac{dp}{dr} = -\frac{\mu \mathbf{K}^{-1} q}{2\pi \rho r h}, \quad (39)$$

where r is the radius of the reservoir, q is the mass production, h is the height of the sink cell, and ρ is the fluid density (Chen and Zhang, 2009). After integrating from the wellbore r_w to the reservoir radius r , we obtain:

$$\Delta p = -\frac{\mu \mathbf{K}^{-1} q}{2\pi \rho h} \ln \left(\frac{r}{r_w} \right), \quad (40)$$

which coincides to the Peaceman well model considering isotropic permeabilities, square grid, single-phase flow, and the well located at the center of an interior cell (Peaceman, 1978). Therefore, we are able to estimate the pressure drop between any location in the reservoir and the sink cell by Eq. (40). Figure 7 shows the pressure distribution inside the reservoir presented in Fig. 6 as a function of the diameter, where we can note that the pressure approximation for the reservoir cells matches the reference solution (real reservoir pressure), while the central cell presents the greatest contribution to the discrepancies due to the well modeling approximation.

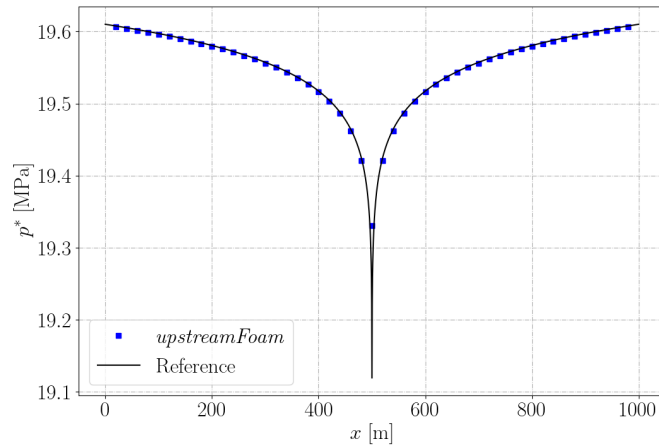


Figure 7: Pressure distribution inside the 2D reservoir as a function of the diameter.

Once a fixed pressure is applied at the boundaries, the numerical head loss of the system can be computed by using the pressure value in the producer cell. In order to obtain a theoretical head loss of 0.49 MPa, we set in Eq. (40) the values of $h = 1$ m and $r_w = 0.1$ m. We remark that in this experiment a value of $r = 500$ m is considered. Table 5 reports the average error between the numerical pressure obtained by the *upstreamFoam* and the reference at time $t = 182.64$ days considering different grid sizes, with $\Delta x = \Delta y$. The results show that with the proposed solver it is possible to obtain accurate estimates of head loss with low errors when compared to the theoretical values.

To indicate the potential of the code, the computational efficiency in this

Cells [-]	Δx [m]	Error [%]	Execution time [s]	Efficiency [%]
489	40.7	0.077	0.63	-
2053	19.6	0.025	1.51	175.16
8021	9.90	0.008	4.7	125.52
31757	4.08	0.005	19.97	93.18
126309	2.49	0.003	84.26	94.26

Table 5: Average errors and execution times according to the grid size for the incompressible case.

two-dimensional case was calculated using the following estimate

$$e_j = \frac{n_j/n_{j-1}}{t_j/t_{j-1}} 100\%, \quad (41)$$

where n_j indicates the number of cells and t_j the execution time for the j -th mesh. The execution times lead to a computational average efficiency of 122.03%, that represents an excellent scalability rate. The efficiency evaluation is not present for the one-dimensional cases because 1D configurations are less suitable for evaluating the performance of the solver.

Lastly, for the same scenario, we estimate the numerical head loss of a compressible oil flow, whose density is given by

$$\rho = \frac{\rho_{o,s} + R_s \rho_{g,s}}{B_{ob} (1 - c_o (p - p_b))}, \quad (42)$$

where $\rho_{o,s}$ and $\rho_{g,s}$ are the densities of oil and gas at standard conditions, R_s is the gas solubility in oil, B_{ob} is the formation volume factor at the bubble point pressure p_b , and c_o is the oil compressibility. Results at time $t = 182.64$ days for $\rho_{o,s} = 880 \text{ kg/m}^3$, $\rho_{g,s} = 1 \text{ kg/m}^3$, $R_s = 199.0$, $B_{ob} = 1.4887$, $p_b = 14.71 \text{ MPa}$, and $c_o = 1.77 \times 10^{-9} \text{ Pa}^{-1}$ are shown in Table 6. We can observe accurate estimates for the numerical pressure, with the errors decreasing as the mesh is refined in the same behavior that the obtained in the incompressible case. The computational time is increased in a proportion such that an average efficiency of 128.26% is attained.

4.2.2. Gas-oil flow in a heterogeneous reservoir

Petroleum reservoirs present high contrast in many proprieties, which impacts the accuracy of the numerical solution and production estimates.

Cells [-]	Δx [m]	Error [%]	Execution time [s]	Efficiency [%]
489	40.7	0.077	0.71	-
2053	19.6	0.026	1.56	187.82
8021	9.90	0.008	5.05	116.35
31757	4.08	0.006	21.13	102.22
126309	2.49	0.003	88.39	106.65

Table 6: Average errors and execution times according to the grid size for the compressible case.

This experiment solves a high-contrast heterogeneous reservoir problem with realistic data provided by the SPE10 benchmark (Christie and Blunt, 2001).

We select the first model, which consists of a two-phase flow (gas and oil) in a 2D vertical cross-sectional geometry whose dimensions are 762 meters long by 7.62 meters wide by 15.24 meters thick, with $100 \times 1 \times 20$ computational cells. The permeability field of the model is shown in Fig. 8, where the x-axis is plotted using a scale of 0.1 in order to obtain an easily readable representation.

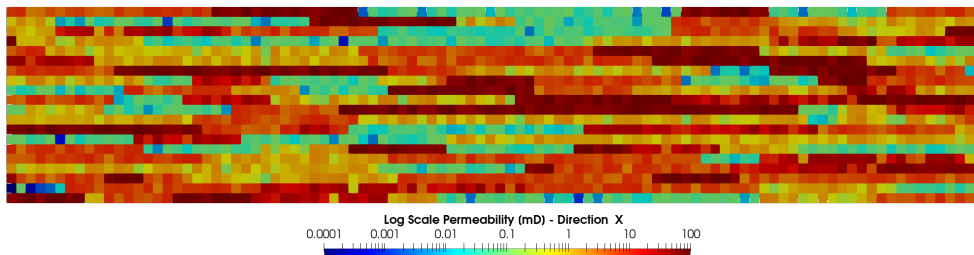


Figure 8: Log-scaled permeability field of the SPE10 project.

An injection-production scenario is considered, where the gas is injected at the left side of the domain (fully saturated with oil), and oil is produced at the right side. Both phases are considered incompressible, while the formation has a compressibility of $c_v = 6 \times 10^{-10} \text{ Pa}^{-1}$ modeled by the linear method with a reference pressure of 689.476 kPa, which is the initial pressure at the top of the model at point 0.0 m. The initial void fraction is $\alpha_v = 0.2$.

The model considers a residual oil fraction of 0.04, that is formulated as a stationary phase fraction in the OpenFOAM framework. Relative permeabilities, illustrated in Fig. 9, are given by the authors in a table. The fluid properties are taken from the SPE10 dataset, that considers the den-

sities $\rho_o = 700 \text{ kg/m}^3$ and $\rho_g = 1 \text{ kg/m}^3$, and viscosities $\mu_o = 0.001 \text{ Pa} \cdot \text{s}$ and $\mu_g = 0.00001 \text{ Pa} \cdot \text{s}$. A constant injection rate of $8.0671 \times 10^{-5} \text{ m}^3/\text{s}$ was applied, along with a production at a constant pressure of 655.002 kPa . In this experiment, capillary effects are neglected, and the Courant time step control is selected with $C_{\max} = 0.5$.

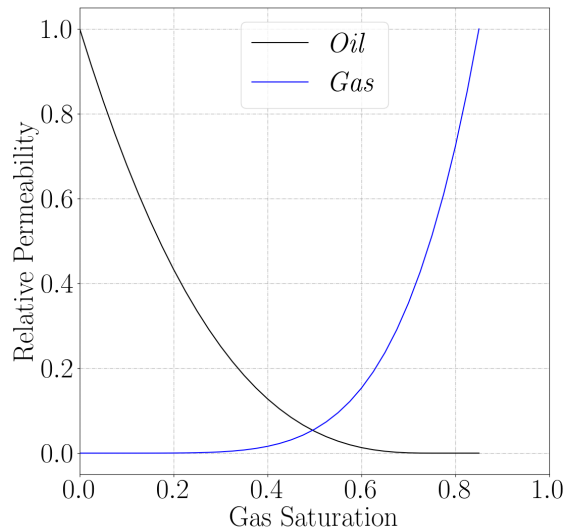


Figure 9: Relative permeabilities for the SPE10 project.

The gas saturation profile after 4800 days can be seen in Fig. 10, where we can note how it flows through the heterogeneous medium. It is possible to observe that gas flows mainly in the superior part of the porous media. This behavior can be justified by the permeability field, presented in Fig. 8.

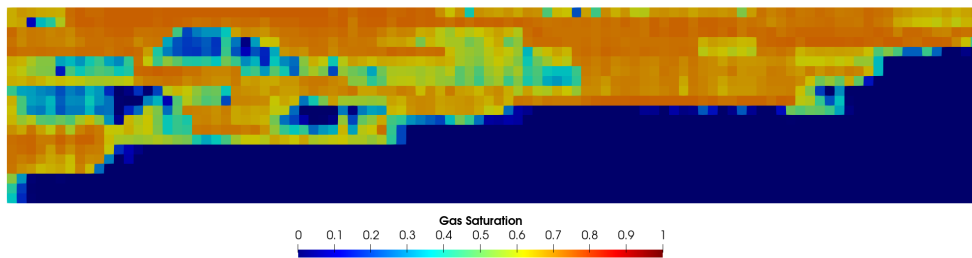


Figure 10: Gas saturation profile after 4800 days.

Figure 11 illustrates the cumulative oil production over a 21-year period (7665 days). The reference result from Landmark (Christie and Blunt, 2001), obtained using the VIP simulator, is used for comparison. At the initial stages, *upstreamFoam* exhibits excellent agreement with the reference result. However, after approximately 500 days, *upstreamFoam* begins to underestimate the cumulative oil production. By 4000 days, it transitions to overestimating the production compared to Landmark’s result. This discrepancy can be attributed to the well injector model, which applies a uniform flow rate across all corresponding cells. It is important to note that well-bore modeling falls outside the scope of this paper; however, it represents a potential avenue for further development and exploration by the authors. More specifically, ongoing work includes the implementation of a Peaceman well model that considers permeability in each cell and can induce actual reservoir productivity. This implementation will then serve as the basis for the development of improved models designed to simulate flows within wells with smart completions, taking into account localized head losses due to different equipment. With the new features, the solver will be able to generate enhanced predictions of well injectivity or productivity, impacting directly the practical decisions in production scenarios.

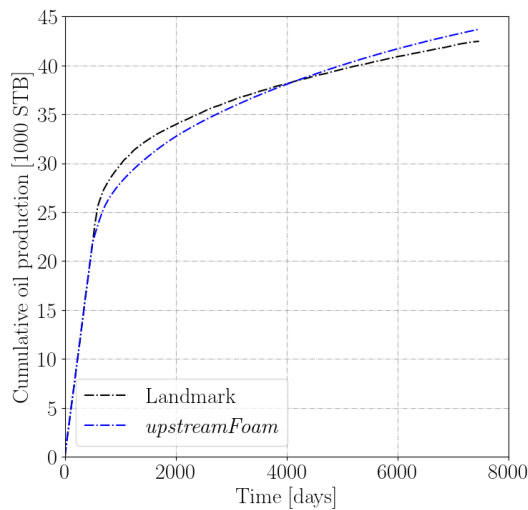


Figure 11: Cumulative oil production.

4.3. Application in a 3D heterogeneous core

Numerical simulations of core flooding experiments are commonly used to validate measurements of rock properties. Therefore, the numerical section is closed with an application of the *upstreamFoam* in a 3D heterogeneous core simulation.

We consider a manufactured core with a relatively Gaussian distribution of the permeability field, as shown in Fig. 12. The domain, with 25 917 computational cells and dimensions of $0.05 \text{ m} \times 0.05 \text{ m} \times 0.106 \text{ m}$, has a homogeneous porosity of $\alpha_v = 0.2$. The core is saturated with oil and water is injected from left at a constant volumetric rate of $1.66 \times 10^{-8} \text{ m}^3/\text{s}$, and the pressure at right is fixed in 0.1 MPa.

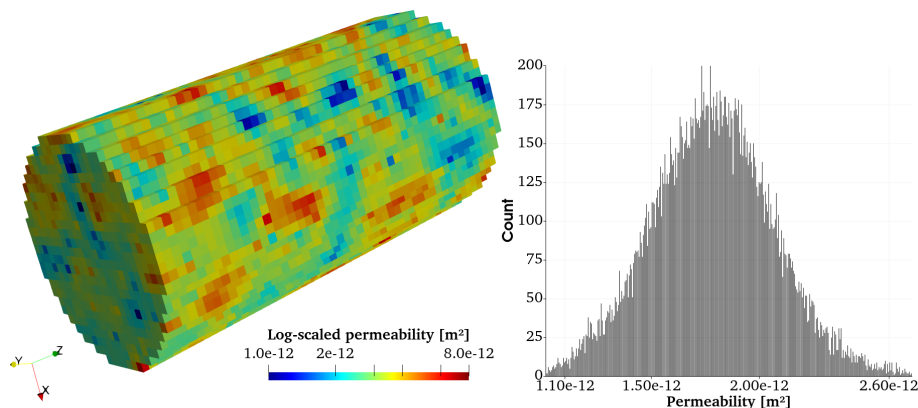


Figure 12: Permeability field of the manufactured core.

In this experiment, gravity and compressibility are neglected. The phase densities are $\rho_w = 1009 \text{ kg/m}^3$ and $\rho_o = 800 \text{ kg/m}^3$, while the viscosities are $\mu_w = 0.0005 \text{ Pa} \cdot \text{s}$ and $\mu_o = 0.002 \text{ Pa} \cdot \text{s}$. We first consider a case without capillary pressure and set the Brooks and Corey relative permeability model with $n = 1$ and $k_{r,i(\max)} = 1$ for both phases. The Coats time step control with $C_{\max} = 0.75$ is selected.

The approximations provided by the *upstreamFoam* and the reference solver *impesFoam* (Horgue et al., 2015) with an equivalent numerical setup are compared. Figure 13 illustrates saturation profiles obtained by both solvers after 2000 s, showing very similar behaviors. For this experiment, the computational time required by *upstreamFoam* was 78.12 s, while *impesFoam* needed 30.11 s.

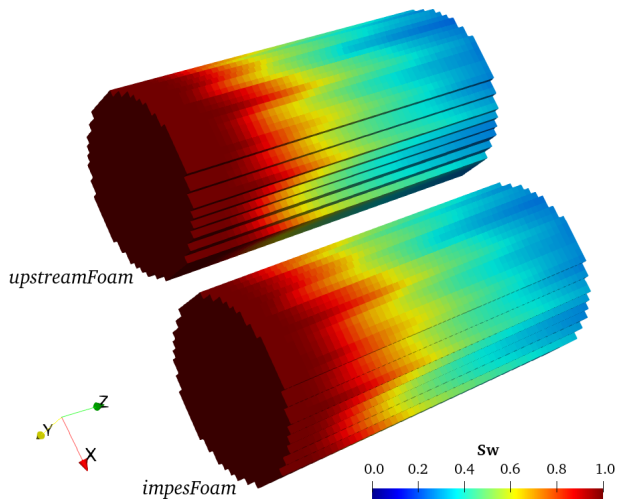


Figure 13: Water saturation profile after 2000 s.

As an illustration of the applicability of the *upstreamFoam* to more complex systems, we consider the previously test in a three-phase scenario with the oil divided into two phases. The core is initialized with saturation of 0.5 for each oil phase, that share the same fluid properties. The saturations at the center line across the core of the established three-phase flow and previous two-phase flow are presented in Fig. 14. The *upstreamFoam* produces the same water saturation for both two and three-phase flow regimes, demonstrating consistent results for the same flow condition, independent from the number of phases. We can also confirm that the saturations of both oil phases are equal. In the referred figure, the *impesFoam* approximation for the two-phase flow is included, which is comparable to the *upstreamFoam* solution. We emphasize that *impesFoam* only considers two-phase flows, therefore, the same test with more mobile phases cannot be carried out on it. This study shows that our two-phase flow solution is in agreement with the produced by a reference solver as well as the capability of the *upstreamFoam* to handle more mobile phases.

Our last experiment presents a qualitative study of the *upstreamFoam* approximation for a case with capillary pressure and more realistic relative permeability curves by comparing our numerical results to the *impesFoam* solution at equivalent conditions. We consider the same two-phase flow in the 3D core geometry and set the Brooks and Corey model for relative permeability with $n = 2$ and $k_{r,i(\max)} = 1$ for both phases. The Brooks and Corey

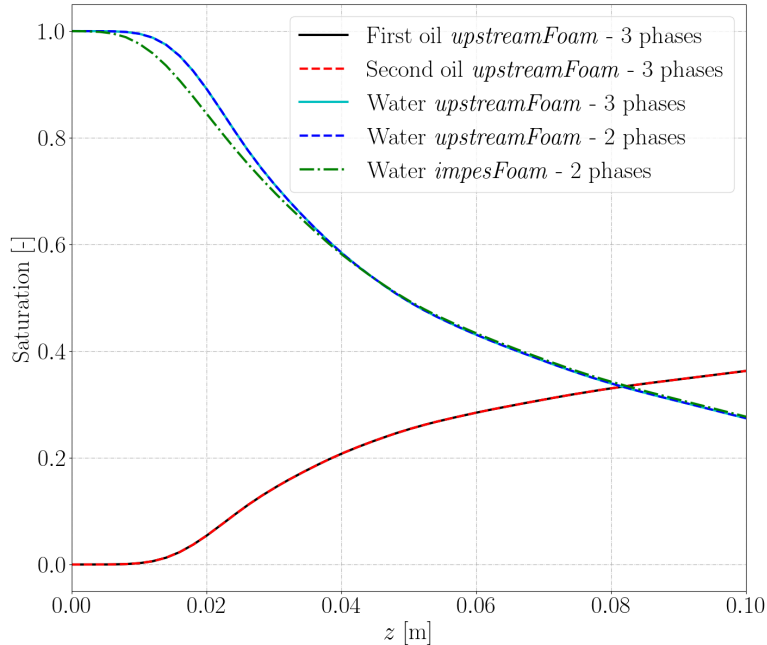


Figure 14: Saturations at 1000s in a center line across the core.

model for the capillary pressure with $\beta = 0.5$ and $p_{c,0} = 10$ Pa is chosen.

Figure 15(a) shows that the simulations performed with *upstreamFoam* and *impesFoam* develop similar saturation profiles. The computational times required by *upstreamFoam* and *impesFoam* were 5.99 h and 2.29 h, respectively. Again, it is important to highlight that despite the *impesFoam* having a significantly lower computational cost, it presents a very limited number of applications when compared to *upstreamFoam*. The same time step Coats restriction has been set for both solvers, which presented similar time step histories, as reported in Fig. 15(b). We remark that the restricted time step sizes presented are close related to the capillary effects, that in this case are not too strong due to the choice of $p_{c,0}$. Other temporal discretizations, such as implicit treatments, can be considered to overcome such limitations.

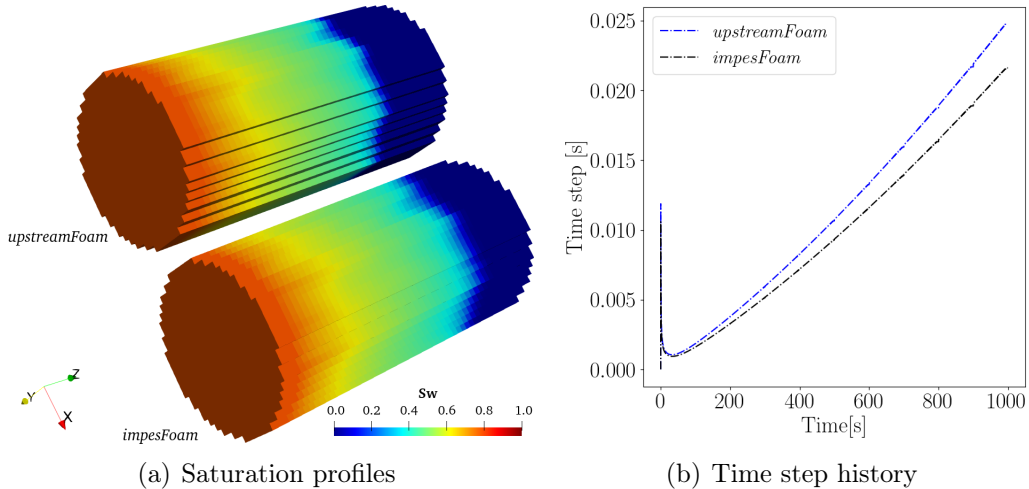


Figure 15: Water saturation profile after 1000s and time step history for the case with capillary pressure and quadratic relative permeability curves.

5. Conclusions

In this work, we introduced and tested a new OpenFOAM application to simulate multiphase flows in porous media. The solver, called *upstreamFoam*, combines the Eulerian multi-fluid formulation for a system of phase fractions with Darcy’s law for flows through porous media. It is based on the *multiphaseEulerFoam* and includes models for reservoir simulation of the *porousMultiphaseFoam*, taking advantage of the most recent technologies developed for these well-established solvers.

The *upstreamFoam* has been successfully tested in a wide range of multiphase flows in porous media. We verified the solver simulating classical problems with analytical, semi-analytical, and reference solutions given by the *porousMultiphaseFoam*. Studies with different data and geometries have been performed to evaluate reservoir properties estimates, resulting in satisfactory accuracy. We also have demonstrated the potential of the solver to approximate complex problems in a multiphase scenario with more than two mobile phases.

The presented solver was developed in a general formulation, that can be extended to multiple species, mass transfer, and others complexities employing the tool-set, capabilities, and efficiency offered by the OpenFOAM framework. In future works, we intend to prepare the code for public release,

include wellbore models, and investigate the use of new schemes to overcome the time step restrictions.

Acknowledgments

The authors would like to thank PETROBRAS (grant 2017/00610-4) for the financial and material support.

References

- Aziz, K., 1979. Petroleum reservoir simulation. Applied Science Publishers 476.
- Bear, J., 1988. Dynamics of fluids in porous media. Courier Corporation, New York.
- Brinkman, H. C., 1949. A calculation of the viscous force exerted by a flowing fluid on a dense swarm of particles. *Flow, Turbulence and Combustion* 1 (1), 27–34.
- Brooks, R. H., 1965. Hydraulic properties of porous media. Ph.D. thesis.
- Carrillo, F. J., Bourg, I. C., Soulaine, C., 2020. Multiphase flow modeling in multiscale porous media: An open-source micro-continuum approach. *Journal of Computational Physics: X* 8, 100073.
- Chen, Z., Huan, G., Ma, Y., 2006. Computational methods for multiphase flows in porous media. SIAM, Philadelphia, PA.
- Chen, Z., Zhang, Y., 2009. Well flow models for various numerical methods. *International Journal of Numerical Analysis & Modeling* 6 (3).
- Christie, M. A., Blunt, M. J., 2001. Tenth SPE comparative solution project: A comparison of upscaling techniques. *SPE Reservoir Evaluation & Engineering* 4 (04), 308–317.
- Coats, K. H., 2000. A note on IMPES and some IMPES-based simulation models. *SPE Journal* 5 (03), 245–251.
- Coats, K. H., 2003. IMPES stability: Selection of stable timesteps. *SPE Journal* 8 (02), 181–187.

- Courant, R., Friedrichs, K., Lewy, H., 1928. Über die partiellen Differenzengleichungen der mathematischen Physik. *Mathematische annalen* 100 (1), 32–74.
- Crowe, C. T., Schwarzkopf, J. D., Sommerfeld, M., Tsuji, Y., 2012. *Multiphase flows with droplets and particles*. CRC Press - Taylor & Francis Group, Boca Raton, FL.
- Damián, S. M., Nigro, N. M., 2014. An extended mixture model for the simultaneous treatment of small-scale and large-scale interfaces. *International Journal for Numerical Methods in Fluids* 75 (8), 547–574.
- Drew, D. A., Passman, S. L., 2006. *Theory of multicomponent fluids*. Vol. 135. Springer Science & Business Media, Berlin.
- Favero, J. L., Silva, L. F. L., Lage, P. L., 2015. Modeling and simulation of mixing in water-in-oil emulsion flow through a valve-like element using a population balance model. *Computers & Chemical Engineering* 75, 155–170.
- Fioroni, S., Larreteguy, A. E., Savioli, G. B., 2021. An OpenFOAM application for solving the black oil problem. *Mathematical Models and Computer Simulations* 13 (5), 907–918.
- Forchheimer, P., 1901. Wasserbewegung durch boden. *Zeitschrift des Vereines Deutscher Ingenieure* 45 (50), 1781–1788.
- Franc, J., Horgue, P., Guibert, R., Debenest, G., 2016. Benchmark of different CFL conditions for IMPES. *Comptes Rendus Mécanique* 344 (10), 715–724.
- Galeazzo, F. C. C., Garcia-Gasulla, M., Boella, E., Pocurull, J., Lesnik, S., Rusche, H., Bnà, S., Cerminara, M., Brogi, F., Marchetti, F., Gregori, D., Weiß, R. G., Ruopp, A., 2024a. Performance comparison of CFD microbenchmarks on diverse HPC architectures. *Computers* 13 (5), 115.
- Galeazzo, F. C. C., Weiß, R. G., Lesnik, S., Rusche, H., Ruopp, A., 2024b. Understanding superlinear speedup in current HPC architectures. Preprints 2024040219.

- Goyeau, B., Lhuillier, D., Gobin, D., Velarde, M., 2003. Momentum transport at a fluid–porous interface. *International Journal of Heat and Mass Transfer* 46 (21), 4071–4081.
- Greenshields, C. J., Weller, H. G., 2022. *Notes on Computational Fluid Dynamics: General Principles*. CFD Direct Ltd, Reading, UK.
- Hill, D. P., 1998. *The computer simulation of dispersed two-phase flow*. Ph.D. thesis, University of London.
- Horgue, P., Renard, F., Gerlero, G. S., Guibert, R., Debenest, G., 2022. porousmultiphasefoam v2107: An open-source tool for modeling saturated/unsaturated water flows and solute transfers at watershed scale. *Computer Physics Communications* 273, 108278.
- Horgue, P., Soullaine, C., Franc, J., Guibert, R., Debenest, G., 2015. An open-source toolbox for multiphase flow in porous media. *Computer Physics Communications* 187, 217–226.
- Ishii, M., Hibiki, T., 2010. *Thermo-fluid dynamics of two-phase flow*. Springer Science & Business Media, New York.
- Jasak, H., 1996. *Error analysis and estimation for the finite volume method with applications to fluid flows*. Ph.D. thesis, Imperial College London (University of London).
- Keser, R., Battistoni, M., Im, H. G., Jasak, H., 2021. A Eulerian multi-fluid model for high-speed evaporating sprays. *Processes* 9 (6), 941.
- Leverett, M., 1941. Capillary behavior in porous solids. *Transactions of the AIME* 142 (01), 152–169.
- Morel-Seytoux, H. J., Meyer, P. D., Nachabe, M., Tourna, J., Van Genuchten, M. T., Lenhard, R. J., 1996. Parameter equivalence for the Brooks-Corey and van Genuchten soil characteristics: Preserving the effective capillary drive. *Water Resources Research* 32 (5), 1251–1258.
- Muskat, M., 1981. *Physical principles of oil production*. McGraw-Hill, New York.

- Nguyen, D. N., Jung, K. S., Shim, J. W., Yoo, C. S., 2022. Real-fluid thermophysical models: An OpenFOAM-based library for reacting flow simulations at high pressure. *Computer Physics Communications* 273, 108264.
- Peaceman, D. W., 1978. Interpretation of well-block pressures in numerical reservoir simulation (includes associated paper 6988). *Society of Petroleum Engineers Journal* 18 (03), 183–194.
- Rudman, M., 1997. Volume-tracking methods for interfacial flow calculations. *International journal for numerical methods in fluids* 24 (7), 671–691.
- Rusche, H., 2003. Computational fluid dynamics of dispersed two-phase flows at high phase fractions. Ph.D. thesis, Imperial College London (University of London).
- Sangnimnuan, A., Li, J., Wu, K., 2021. Development of coupled two phase flow and geomechanics model to predict stress evolution in unconventional reservoirs with complex fracture geometry. *Journal of Petroleum Science and Engineering* 196, 108072.
- Silva, L. F. L., Damian, R., Lage, P. L., 2008. Implementation and analysis of numerical solution of the population balance equation in CFD packages. *Computers & Chemical Engineering* 32 (12), 2933–2945.
- Silva, L. F. L., Lage, P. L., 2011. Development and implementation of a poly-dispersed multiphase flow model in OpenFOAM. *Computers & chemical engineering* 35 (12), 2653–2666.
- Soulaine, C., Tchelepi, H. A., 2016. Micro-continuum approach for pore-scale simulation of subsurface processes. *Transport in porous media* 113, 431–456.
- Spalding, D. B., 1981. Numerical computation of multi-phase fluid flow and heat transfer. In *Von Karman Inst. for Fluid Dyn. Numerical Computation of Multi-Phase Flows*, 161–191.
- Sugumar, L., Kumar, A., Govindarajan, S. K., 2020. Grid adaptation of multiphase fluid flow solver in porous medium by OpenFOAM. *Petroleum & Coal* 62 (4).

- Tocci, F., 2016. Assessment of a hybrid VOF two-fluid CFD solver for simulation of gas-liquid flows in vertical pipelines in OpenFOAM. Master's thesis, Politecnico di Milano, Italy.
- Wang, H., Wang, H., Gao, F., Zhou, P., Zhai, Z. J., 2018. Literature review on pressure-velocity decoupling algorithms applied to built-environment CFD simulation. *Building and Environment* 143, 671–678.
- Wardle, K. E., Weller, H. G., 2013. Hybrid multiphase CFD solver for coupled dispersed/segregated flows in liquid-liquid extraction. *International Journal of Chemical Engineering* 2013.
- Weller, H. G., 2002. Derivation, modelling and solution of the conditionally averaged two-phase flow equations. Nabla Ltd, No Technical Report TR/HGW 2, 9.
- Weller, H. G., 2008. A new approach to VOF-based interface capturing methods for incompressible and compressible flow. OpenCFD Ltd., Report TR/HGW 4, 35.
- Weller, H. G., Tabor, G., Jasak, H., Fureby, C., 1998. A tensorial approach to computational continuum mechanics using object-oriented techniques. *Computers in physics* 12 (6), 620–631.
- Wu, Y.-S., 2015. Multiphase fluid flow in porous and fractured reservoirs. Gulf professional publishing, Waltham, MA.